J. KSIAM Vol.20, No.3, 175–202, 2016 http://dx.doi.org/10.12941/jksiam.2016.20.175

[SPECIAL SECTION : **Mathematics in Industry**]

INDUSTRIAL MATHEMATICS IN ULTRASOUND IMAGING

JAESEONG JANG[1] AND CHI YOUNG AHN[2,†]

[1]DEPARTMENT OF COMPUTATIONAL SCIENCE AND ENGINEERING, YONSEI UNIVERSITY, SEOUL, KOREA
E-mail address: jaeseongj@yonsei.ac.kr

[2]DIVISION OF INTEGRATED MATHEMATICS, NATIONAL INSTITUTE FOR MATHEMATICAL SCIENCES, DAEJEON, KOREA
E-mail address: chiyoung@nims.re.kr

ABSTRACT. Ultrasound imaging is a widely used tool for visualizing human body's internal organs and quantifying clinical parameters. Due to its advantages such as safety, non-invasiveness, portability, low cost and real-time 2D/3D imaging, diagnostic ultrasound industry has steadily grown. Since the technology advancements such as digital beam-forming, Doppler ultrasound, real-time 3D imaging and automated diagnosis techniques, there are still a lot of demands for image quality improvement, faster and accurate imaging, 3D color Doppler imaging and advanced functional imaging modes. In order to satisfy those demands, mathematics should be used properly and effectively in ultrasound imaging. Mathematics has been used commonly as mathematical modelling, numerical solutions and visualization, combined with science and engineering. In this article, we describe a brief history of ultrasound imaging, its basic principle, its applications in obstetrics/gynecology, cardiology and radiology, domestic-industrial products, contributions of mathematics and challenging issues in ultrasound imaging.

1. INTRODUCTION

Ultrasound imaging system visualizes organs inside human body using sound waves with the frequency range of $1\sim15\ MHz$ higher than human audible frequency. Due to the various advantages of non-invasiveness, safety, portability(see Fig. 1), relatively low cost and real-time imaging over other imaging modalities such as CT and MRI, it is widely used in various diagnostic fields of obstetrics and gynecology, cardiology, radiology, and so on.

Recently, it was reported that ultrasound market size was growing and the ultrasound market including diagnostic ultrasound would be worth about 6.23 billion USD in 2020 [1, 2]. In

Received by the editors August 17 2016; Revised August 28 2016; Accepted in revised form August 29 2016; Published online September 5 2016.

2000 *Mathematics Subject Classification.* 68U10, 92C50.

Key words and phrases. Industrial Mathematics, Ultrasound Imaging, Ultrasound Examinations, Image Processing, Technology Advances, Mathematical Modelling.

† Corresponding author.

FIGURE 1. Ultrasound imaging systems of major companies: GE, Philips, Siemens, Samsung Medison and Alpinion (from their homepages). The three companies of (a)-(c) have over half of global ultrasound market share [3]. The two companies of (d) and (e) are leading domestic companies.

order to have bigger market share, each global company tries to develop competitive imaging technologies and to expand ultrasound use in other applications. For example, one of the most promising technologies affected by increased computational power is real-time 3D ultrasound imaging. It is capable of providing good 3D visualization of organs at the faster rate of about 30 volumes per seconds compared to volumetric imaging modalities such as CT and MRI. However, its resolution is not good enough so that it often fails to discriminate features smaller than a few millimeters. Because of this resolution limitation, real-time 3D ultrasound imaging is not frequently adopted for clinical examinations in radiology. Whereas, it is meaningfully used for observing cardiac wall motion in cardiology or for distinguishing between tissues and surrounding fluids in obstetrics and gynecology. In order to circumvent the resolution problem, each company concentrates on fusion imaging technique that incorporates two images acquired from two different imaging modalities: real-time ultrasound images and CT or MRI images acquired earlier. It is able to provide more anatomical information indistinguishable with the resolution of real-time 3D ultrasound imaging and expand ultrasound use in radiology. As other examples of the promising technologies, we can consider image quality enhancement, faster imaging, 3D color Doppler imaging, computer-aided detection (CADe), computer-aided diagnosis (CADx) and advanced functional imaging modes such as elasticity imaging and vortex flow imaging. They are also very interesting and challenging issues to be improved in ultrasound imaging.

Then how can we advance and innovate ultrasound imaging technologies? Like in other industries, *Mathematics* has played an important role in ultrasound imaging and medical diagnosis already. For acquiring gray-level echo images and color Doppler images, *Mathematics* is used in various parts of time-delay computation for beam-forming, Fourier tranform of ultrasound signal for signal processing or filter design, auto-correlation computation for mean frequency estimation, linear interpolation for scan conversion, and so on [4, 5]. *Mathematics*

is also used to extract functional information from ultrasound images. In order to avoid labor-intensive and time-consuming manual measurements on gray-scale echo images, automated segmentation and motion tracking algorithms are demanded. The automated measurement methods are based on partial differential equation, numerical analysis, statistics as well as the interpretation of acoustic fields and speckles as inherent appearance in ultrasound imaging. Therefore, we can see that various levels of mathematical modelling and methods are applied to acquire ultrasound images and to generate functional information for clinical evaluations.

Moreover, *Mathematics* is essential in cases of elasticity imaging and vortex flow imaging mentioned above. Elasticity imaging is an imaging mode to map the stiffness of soft tissues such as liver or breast, and it can be implemented by reconstructing elastic modulus from measured displacements governed by the elastic equation:

$$\nabla \cdot (\mu(\nabla \mathbf{u} + \nabla \mathbf{u}^t)) + \nabla(\lambda \nabla \cdot \mathbf{u}) = \rho \frac{\partial^2}{\partial t^2}\mathbf{u}, \tag{1.1}$$

where $\mathbf{u}$ denotes the displacement vector, $\nabla \mathbf{u}^t$ the transpose of the matrix $\nabla \mathbf{u}$, ρ the density of the soft tissue as elastic material, μ the shear modulus with $\mu = \frac{E}{2(1+\nu)}$ and λ the Lamé coefficient with $\lambda = \frac{\nu E}{(1+\nu)(1-2\nu)}$. Here, E and ν are Young's modulus and Poisson's modulus, respectively.

Vortex flow imaging is an imaging mode to quantify the vorticity of intra-ventricular blood flows and to offer possible clinical indices. Since the vorticity fields are obtained by taking the curl operator to velocity fields of flows, the velocity fields should be exactly computed. The velocity fields can be computed by solving the Navier-Stokes equation:

$$\begin{cases} \tilde{\rho}\left(\dfrac{\partial \mathbf{v}}{\partial t} + \mathbf{v} \cdot \nabla \mathbf{v}\right) = -\nabla p + \tilde{\mu}\nabla^2 \mathbf{v} & \text{in } \Omega_t, \\ \nabla \cdot \mathbf{v} = 0 & \text{in } \Omega_t, \end{cases} \tag{1.2}$$

where Ω_t denotes the intra-ventricular domain varying within the heartbeat cycle T, $\mathbf{v}$ the velocity fields, $\tilde{\rho}$ the blood density and $\tilde{\mu}$ the blood viscosity.

The displacements of soft tissues and the motion of blood flows are understood through physics-based mathematical modelling using elastic and fluid equations. Under those mathematical models, we deal with measurements obtained through ultrasound imaging systems, construct the overall phenomenon from the partially measured data and quantify clinically meaningful information. The point is that ultrasound imaging technologies will be advanced and innovated through *Mathematics*.

The aim of this paper is to describe the importance and value of *Mathematics* in ultrasound imaging and to share them with other scientists and engineers. In this paper, we describe a brief history of ultrasound imaging, basic imaging principle, its applications in major diagnostic fields, domestic-industrial products and contributions of mathematics, especially for beginners to understand ultrasound imaging and pay much attention to it. Furthermore, we introduce hot topics and challenging issues related to ultrasound imaging. They have to be resolved for the advancements of ultrasound imaging technology. We hope many mathematicians recognize how mathematics is used and contributes much to ultrasound technology innovation.

2. The History of Diagnostic Ultrasound Imaging

The history of ultrasound imaging starts with the history of sonar, the abbreviation of SOund Navigation And Ranging, measuring the depth of water using sound wave. In the late 1800s, the theoretic and practical foundation for sonar and ultrasound imaging was established by a mathematical equation describing sound wave and the discovery of piezo-electricity, electricity resulting from pressure. L. Rayleigh described sound wave as a mathematical equation in his paper "the Theory of Sound" published in 1877 and P. Curie and his brother J. Curie discovered the piezo-electric effect in certain crystals in 1880 [6–8].

Since the sinking of the Titanic in 1912 and World War I, echo-ranging systems were demanded to detect icebergs or submarines. In 1917, P. Langevin, one of the Curie brothers' first students developed practical underwater echo-ranging systems using the piezo-electricity for transducer, a device converting a voltage difference to a mechanical stress and reversely converting a mechanical pressure to an electric potential. During World War II, echo-ranging technique was applied to electromagnetic waves and became radar, the abbreviation of RAdio Detection And Ranging.

Echo-ranging system as a diagnostic device to probe the human body was not developed until the 1940's. K. Dussik used ultrasound to diagnose brain tumor by transmitting an ultrasound beam through the human skull in 1942 [6, 7, 9]. He is regarded as the first-time user of ultrasound for medical diagnosis. In 1948, G. Ludwig used A-mode ultrasound system to detect gallstones [7, 10]. The A-mode shows a signal profile representing the instantaneous echo signal amplitude over time after transmission of the acoustic pulse.

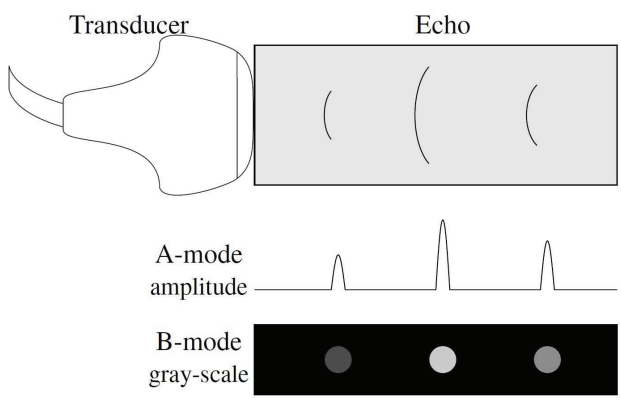

Figure 2. Illustration of the A-mode and B-mode displays. A 2D B-mode image consists of multiple and sequential B-mode lines.

After that time, innovative advances of ultrasound imaging technologies have followed. In the 1950s, 2D B-mode ultrasound imaging system was developed and applied to detect breast tumors and to diagnose in the obstetrics and gynecology fields [6, 11]. The B-mode represents the brightness converted from the amplitude of the echo signals. Fig. 2 illustrates the A-mode and B-mode displays.

Since the first implementation of ultrasonic Doppler techniques in Japan in 1955 [12], various Doppler techniques including the continuous wave Doppler, spectral wave Doppler, and color Doppler ultrasound were developed through the 1960s and the 1970s [7, 13–17]. The emergency of 3D ultrasound technology in the 1980s was capable of capturing 3D images of a fetus [18, 19]. Thanks to the continuous improvements of image quality and 3D imaging capabilities, ultrasound technology became more sophisticated and capable of real-time 3D imaging in the 1990s [20].

From the 2000s to present, 2D arrays of transducers were used for real-time 3D imaging, ultrasound imaging system became miniaturized gradually and ultrasound imaging technology is developing steadily for improving image quality, reducing costs, reducing exam times and being applied to wider diagnostic areas. Recently, hand-carried systems became available. It is becoming common with significant growth and can be used for clinical assessments even in developing countries [21, 22] due to the portability and low cost in addition to higher image quality obtained by using special ultrasound probes for transesophageal echocardiography and transverginal echo [23, 24].

More detailed information about the history of ultrasound imaging can be found at the references [4, 6].

3. Basic Principle of Ultrasound Imaging

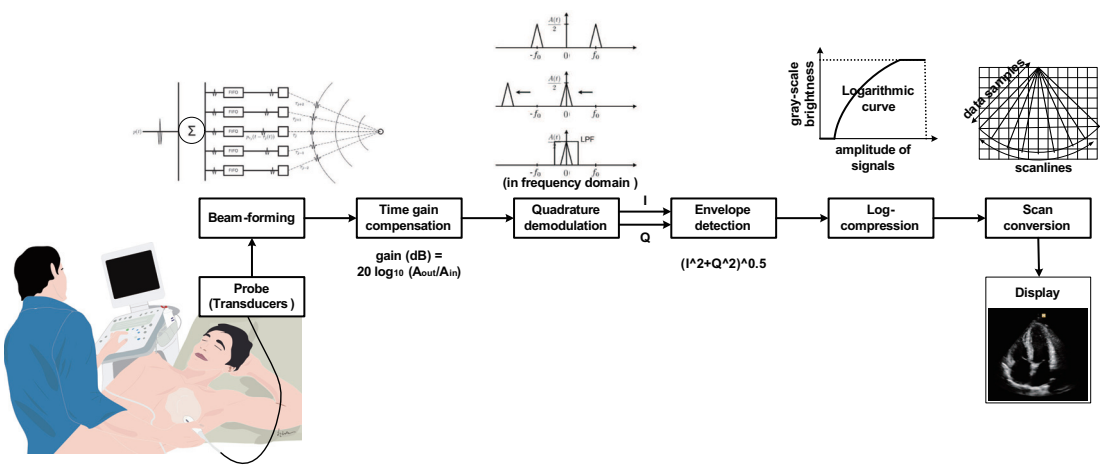

FIGURE 3. Block diagram of ultrasound B-mode imaging.

In this section, we describe the basic principle of ultrasound imaging, especially focusing on gray-scale echo images, called the B-mode images. Fig. 3 shows intuitively that mathematics, combined with science and engineering, is used in the process of ultrasound B-mode imaging. Furthermore, we deal with the mathematical models on acoustic fields, fundamental in ultrasound imaging, and describe their applications. We can see that mathematics is applied usually as mathematical modelling, numerical solutions and visualization.

3.1. **Ultrasound B-mode imaging.** An ultrasound image consists of several sequential scanlines (around $128 \sim 512$ scanlines), each of which is usually acquired through transmission and reception beam-forming using transducer arrays. The transmission beam-forming is to control electronically time delays for ultrasound beam emitted from the transducer arrays to be focused at a point on each scanline. The reception beam-forming is to control electronically time delays to accumulate back-scattered echo signals from a specific position, called the received focal point, on scanlines. We note that the received focal point can be changed dynamically on each scanline.

As sound travels through a material, the amplitude or intensity is decreased due to three factors: absorption, scattering and beam divergence. We start describing mathematically the ultrasound imaging principle, together with beam-forming, considering the time gain compensation of the received and beam-formed echo signals [25, 26].

3.1.1. *Beam-forming and gain compensation.* Let N be the number of transducers, $\mathbf{r}_j$ the position of the j-th transducer and p_j the received signal at $\mathbf{r}_j$ for $j = 1, \cdots, N$. We assume that transducers are very small, sample positions on each scanline are far away from the transducers and the impulse response is given in the form of Dirac delta function. Then, for sample position $\mathbf{r} = (x, y, z)$ on a given scanline, the amplitude of the received signal at time t is expressed as

$$p(t) = \sum_{j=1}^{N} p_j(t - \tau_j) = K \sum_{j=1}^{N} \delta\left(t - \frac{|\mathbf{r}_j - \mathbf{r}|}{c}\right), \tag{3.1}$$

where τ_j is the delayed time and K a constant depending on depth.

3.1.2. *Quadrature demodulation and envelope detection.* Let f_0 be the center frequency of transmission signals. Then the amplitude (3.2) of the beam-formed signal along the given scanline can be expressed as

$$\begin{aligned} p(t) &= a(t)\cos(2\pi f_0 t + \phi(t)) \\ &= \frac{a(t)}{2}\left(e^{i(2\pi f_0 t + \phi(t))} + e^{-i(2\pi f_0 t + \phi(t))}\right), \end{aligned} \tag{3.2}$$

where $a(t)$ and $\phi(t)$ are the amplitude and the phase of the received signal, respectively. In order to remove signals with high-frequency and obtain meaningful signal with low-frequency, we perform the quadrature demodulation. By setting $\hat{p}(t) = p(t)e^{-2\pi f_0 t}$ and applying a low-pass filter to $\hat{p}(t)$, we can obtain a base-band complex signal $\frac{a(t)}{2}e^{i\phi(t)}$. Its real and imaginary parts are called In-phase and Quadrature signals, denoted by $I(t)$ and $Q(t)$, respectively.

$$\begin{aligned} I(t) &= \mathfrak{Re}\left(\frac{a(t)}{2}e^{i\phi(t)}\right), \\ Q(t) &= \mathfrak{Im}\left(\frac{a(t)}{2}e^{i\phi(t)}\right). \end{aligned} \tag{3.3}$$

After the envelope detection by taking $\sqrt{I(t)^2 + Q(t)^2}$ from the quadrature demodulated signals $I(t)$ and $Q(t)$, logarithmic compression follows.

3.1.3. *Logarithmic compression.* Most of clinically meaningful signals are appeared with the small value in the wide range of amplitude. The logarithmic compression is required to display these meaningful signals in the 256 gray-scale values. The image intensity $I(t)$ is expressed as

$$I(t) = \frac{I_{max} - I_{min}}{\ln A_{max} - \ln A_{min}} \ln\left(\frac{A(t)}{A_{min}}\right) + I_{min}, \tag{3.4}$$

where I_{max} and I_{min} are the maximum and minimum intensity values, to be displayed finally in the gray-scale, respectively, and A_{max} and A_{min} the maximum and minimum amplitude values with the range of interest, respectively.

3.1.4. *Digital scan conversion and display.* These intensity values at the sample positions along each scanline are displayed on a video screen through scan conversion process for the spatially arrangement. Scan conversion is performed by using bi-linear interpolation.

In order to improve the B-mode image, some signal/image processing methods may be used additionally.

3.2. **Acoustic fields.** Jensen [27] derived an inhomogeneous wave equation describing the propagation and scattering of ultrasound in an inhomogeneous medium, derived a mathematical model for the received pulse-echo pressure fields by considering the surface shape of a single transducer element used in diagnostic ultrasound and showed simulated pressure field compared to a measured field. In this subsection, we describe the mathematical models and their applications.

3.2.1. *Mathematical modelling.* Let $p(\mathbf{r}, t)$ be the pressure variation caused by ultrasound propagation at the position $\mathbf{r}$ and time t, $c(\mathbf{r})$ the propagation speed and $\rho(\mathbf{r})$ the material density. Then the inhomogeneous wave equation is derived as

$$\nabla^2 p - \frac{1}{{c_0}^2}\frac{\partial^2 p}{\partial t^2} = -\frac{2(\delta c)}{{c_0}^3}\frac{\partial^2 p}{\partial t^2} + \frac{1}{\rho_0}\nabla(\delta\rho)\cdot\nabla p, \tag{3.5}$$

where c_0 is the mean propagation speed, ρ_0 the mean density, δc the speed variation from c_0 and $\delta\rho$ the density variation from ρ_0.

Let $p_r(t)$ the received signal at the transducer surface and $E_m(t)$ at time t. Then $p_r(t)$ is written as

$$p_r(t) = \frac{\rho_0}{2{c_0}^2}E_m(t) \underset{t}{*} \frac{\partial^3 v(t)}{\partial t^3} \underset{t}{*} \left[\left(\frac{\delta\rho(\mathbf{r})}{\rho_0} - \frac{2(\delta c(\mathbf{r}))}{c_0}\right) \underset{\mathbf{r}}{*} H(\mathbf{r}, t)\right], \tag{3.6}$$

where $\underset{t}{*}$ and $\underset{\mathbf{r}}{*}$ mean the time convolution and spatial convolution, respectively. Note that $\frac{\rho_0}{2{c_0}^2}E_m(t) \underset{t}{*} \frac{\partial^3 v(t)}{\partial t^3}$ is the pulse-echo including the transducer excitation and the electromechanical impulse response during the emission/reception of the pulse, $\frac{\delta\rho(\mathbf{r})}{\rho_0} - \frac{2(\delta c(\mathbf{r}))}{c_0}$ is the inhomogeneities in tissue and $H(\mathbf{r}, t)$ is the pulse echo spatial impulse response given by $H(\mathbf{r}, t) = h(\mathbf{r}, t) \underset{t}{*} h(\mathbf{r}, t)$ with $h(\mathbf{r}, t) = \int_S \frac{\delta(t - |\mathbf{r} - \mathbf{r}_0|/c_0)}{2\pi|\mathbf{r} - \mathbf{r}_0|} d\mathbf{r}_0$ for the transducer surface S.

For validating the derived mathematical model (3.6), a simulation was performed under the setup that a plane reflector was placed at focal point. According to an excited Dirac impulse,

impulse responses were computed at the distances of three different positions from transducer surface and compared to measured responses.

3.2.2. *Field II simulation program.* Afterward Jensen [28, 29] improved the mathematical model (3.6) for the propagation and scattering of acoustic fields by considering acoustic fields from arbitrarily shaped, apodized and excited transducers and dealing with the imaging principle, and developed a simulation program based on the derived mathematical model and running under MATLAB software. It is called Field II. Using Field II simulation program, we can simulate ultrasound transducer fields and generate some gray-level echo and color Doppler images similar to real ultrasound images acquired in ultrasound imaging system as depicted in Fig. 4. Field II is widely used in several companies, universities and departments because

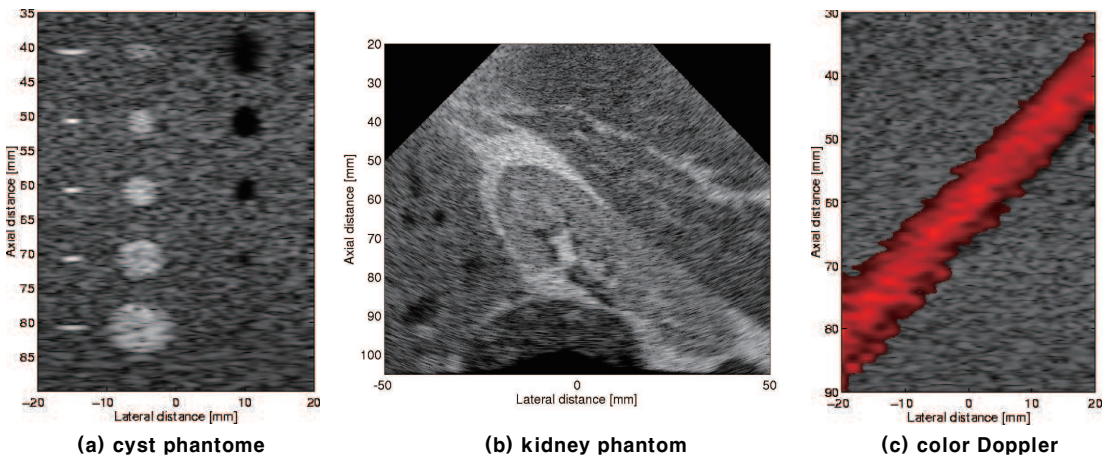

FIGURE 4. Examples of ultrasound synthetic images generated by using Field II.

it is very helpful for scientists and engineers to understand ultrasound imaging and study image processing methods such as speckle reduction on the synthetic images. It is available at: http://field-ii.dk/.

4. APPLICATIONS OF DIAGNOSTIC ULTRASOUND IMAGING

Thanks to the advanced imaging technologies such as image quality enhancement, real-time 3D imaging and the miniaturization of equipment, ultrasound is widely applied to various diagnostic fields of obstetrics and gynecology(OB/GYN), cardiology, radiology, urology, and so on. We note that applications in OB/GYN, cardiology and radiology account for about 70% of the entire ultrasound examinations. In this section, we provide brief explanations of ultrasound imaging applications in major three diagnostic areas.

4.1. **OB/GYN ultrasound.** Since the 1950's, ultrasound has been used for the diagnosis of gestation and women's health. The ultrasound market for OB/GYN examinations has continued to increase. The main issues of ultrasound imaging in OB/GYN is to improve the image quality for detecting endometriosis and gynecological cancer, diagnosing early miscarriage and ectopic pregnancy, and evaluating fetal growth. Especially the performance enhancement of static and real-time 3D imaging is still a hot issue for easier detection of fetal abnormalities in obstetrics.

4.1.1. *Ultrasound examinations.* Fetal ultrasound examinations are classified into four parts: first-trimester examination, standard second- or third-trimester examination, limited examination and specialized examinations [30]. Most of the examinations performed by observing or measuring target objects: the presence, size, location and number of gestational sac(s), fetal presentation, amniotic fluid volume, cardiac activity, placental position, fetal biometry, fetal heart activity, and so on.

On the other hand, gynecological examinations such as the detection of endometriosis and gynecological cancer are performed commonly by transvaginal scans, with the probe designed to be placed in the vagina of patient. Since the scanhead of the probe is closely adjacent to uterus, the transvaginal scans provide better image qualities and are useful for the early diagnosis of miscarriage and ectopic pregnancies.

Recent advances of static and real-time 3D ultrasound imaging through various image processing and volume rendering techniques have enabled performing more accurate diagnosis for ectopic pregnancy [31] and providing more accurate diagnostic information: abnormalities and anomalies by visualizing fetal face, brain, spine, and skeleton [32], fetal weight obtained by measuring abdominal, thigh, arm volumes and head circumference [33–35], and the volumes of lung and heart [36, 37]. High quality images and accurate boundary extraction are required for fetal examinations.

In addition, Doppler ultrasound is indispensable for detecting fetal heartbeat as well as blood flow characteristics in the various fetal blood vessels: umbilical artery, aorta, middle cerebral arteries, uterine arcuate arteries and inferior vena cava. Power or color Doppler images are used for examinations of fetal middle cerebral artery and cerebral venous [38, 39]. Blood flow to fetus through umbilical cord is also observed by color Doppler images [40, 41]. Note that color Doppler images reflect one-directional velocity components of blood flow along scanlines and power Doppler shows the volume of blood, rather than its velocity.

4.1.2. *Innovative technologies for OB/GYN.* Samsung Medison, a leading domestic company, has released recently a premium ultrasound system 'WS80A with Elite' with superior ultrasound imaging techniques for OB/GYN examinations: *S-Harmonic*, ClearVision™, Realistic Vue™, *Crystal Vue*, etc. Among them, we pay attention to *Crystal Vue* an advanced rendering technique to enhance the image contrast of 3D volume data. It is capable of imaging the interface of bone and soft tissue with high accuracy and providing intuitive information on the contour of fetal skeleton, face and brain. Lately, *Crystal Vue* has been featured on the front cover of Ultrasound in Obstetrics & Gynecology (UOG), a renowned journal in the women's

healthcare industry [42]. The images of fetal spine and ribs obtained by *Crystal Vue* were selected as the Picture of the Month by UOG. They provide remarkably clear and realistic information of fetal spine and ribs.

Together with the advanced rendering technique, ElastoScan™ for gynecology is also being promoted. It is used to diagnose benign gynecological disorders and to differentiate uterine fibroids and adenomyosis. We can appreciate the remarkable images acquired by Samsung Medison's innovative imaging technologies at: http://www.samsungmedison.com/ultrasound/ob-gyn/ws80a-with-elite/.

4.2. **Cardiological ultrasound.** Due to the high temporal resolution of ultrasound imaging, cardiac ultrasound (echocardiography) has been very successful in providing a quick assessment of the overall health of heart, a very fast moving complex organ positioned deep within the body. Ultrasound examinations of heart functions related to cardiac wall motion, valve motion and blood flow are performed by various ultrasound imaging modes: gray-scale imaging, tissue Doppler imaging, color Doppler imaging and real-time 3D imaging. Note that tissue Doppler images represent the velocity of cardiac wall motion.

4.2.1. *Ultrasound examinations.* Echocardiographic examinations include numerous diagnosing items: valvular heart disease, hypertensive heart disease, ischemic heart disease, cardiac tumors, evaluation of the left and right atrium, evaluation of left ventricle(LV) systolic/diastolic function, congenital heart disease, diseases of the aorta, and so on. For more detailed description on echocardiographic examinations, we refer to the literature 'The Echocardiographer's Pocket Reference' by T. Reynolds(2013) [43].

Among echocardiographic examinations, we consider only evaluation of LV function including dimensions, volumes, wall thickness, LV mass, LV mass index, longitudinal motion, radial motion, circumferential, segmental wall motion, wall motion score index, etc. For its quantitative assessment, wall motion tracking and LV volume quantification at each time is needed. To avoid labor-intensive and time-consuming manual LV tracing process, demand for automated LV tracking and analysis methods has been rapidly growing and there have been plenty of studies on LV tracking methods. In Section 6, we represent a problem on LV motion tracking and solutions by mathematical modelling.

4.2.2. *A software for quantifying cardiac function.* Automated LV tracking methods can be applied to analyze and quantify LV function. TomTec is a leading company in medical imaging software solutions and offers industry partners or clinicians various solutions for quantifying cardiac function based on 2D and 3D echocardiography. As an example of software solutions, TomTec developed AutoStrain© by applying automated LV tracking method to visualize LV function quantitatively. AutoStrain© provides automated LV function analysis based on cardiac apical long axis views. It visualizes longitudinal strain results, obtained by 2D speckle tracking, to be color-coded in the individual clips and combined in a Bull's-eye plot.

4.2.3. *A software for visualizing and quantifying blood flows.* On the other hand, another imaging software company AMID has recently developed 'hi-def flow tracking' a software

for visualizing and quantifying the motion of blood flow (http://www.amid.net). It is also called Omega Flow (Siemens, Mountain View, CA). It is not based on color Doppler images, but echo-PIV technique applied to contrast-enhanced echocardiographic images. Along with studies on its clinical possibility and feasibility, this software continues to develop to be used to evaluate cardiac function clinically.

4.3. **Radiological ultrasound.** Ultrasound examinations in radiology consist of abdominal, vascular, musculoskeletal, breast, thyroid ultrasonographies, and so on. Most of ultrasound examinations are performed by observing main features or measuring the shape and size of target objects using gray-scale B-mode images. Doppler ultrasound is used typically for evaluating blood flow through blood vessels.

4.3.1. *Ultrasound examinations.* Abdominal ultrasonography is used for diagnosing the diseases of liver, gallbladder, spleen, pancreas, kidneys and bladder. As an example, liver is scanned to examine focal liver disease, diffuse liver disease and hepatic vasculature.

Vascular ultrasound is adopted typically for observing common/internal carotid artery and diagnosing carotid stenosis and chronic mesenteric ischaemia. According to carotid artery stenosis, gray-scale B-mode images is used for characterizing plaques into four types and Doppler ultrasound is used for evaluating both the macroscopic appearance of plaques and flow characteristics [44].

Musculoskeletal ultrasound is a fast and dynamic way to examine shoulder impingement, shoulder instability and rotator cuff disorders. It also allows evaluation of the joint, tendons and ligaments by imaging elbow anatomy and wrist anatomy. Moreover, it is used for diagnosing hand, hip, knee, ankle/foot, etc.

Breast ultrasound enables evaluating a symptomatic young or pregnant patient, to evaluate a palpable lump with negative or equivocal mammographic findings, and to distinguish between benign and malignant characteristics. Benign characteristics of breast lesions include well-circumscribed and hyperechoic tissue, wider than deep and gently curving smooth lobulation. Meanwhile, malignant characteristics contain sonographic spiculation, deeper (taller) than wide, micro-lobulation, thick hyperechoic halo, angular margins and markedly hypoechoic nodule [45].

Ultrasonography of thyroid is used to diagnose multi-nodular goitre, colloid cyst and thyroglossal duct cyst. Especially for diagnosing intra-nodular vascularity, Doppler ultrasound is required. Large cystic component, comet tail artifact and halo are regarded as benign sonographic features of multi-nodular goitre, while intra-nodular blood flow, large size and presence of micro-calcification are classified as malignant features.

In addition, ultrasound elastography is used for evaluating liver disease or detecting tumors of breast and thyroid by providing additional stiffness information of tissues [46, 47]. Different from the conventional ultrasound imaging modes, it is a relatively new imaging mode for visualizing qualitatively or quantitatively the stiffness information of tissues.

4.3.2. *High technologies for radiology ultrasound.* For radiology examinations, Samsung Medison has released a premium ultrasound system ‘RS80A with Prestige’ with high technologies:

S-Harmonic, *HQ Vision*, NeedleMate™, *CEUS+*, *S-Fusion*, *S-Tracking*, S-Detect™ for Breast, S-Detect™ for Thyroid, *S-Shearwave*, ElastoScan™, etc. We can see the Samsung Medison's high technologies at: http://www.samsungmedison.com/ultrasound/general-imaging/rs80a/.

5. Domestic-Industrial Products and Imaging Technologies

Samsung Medison and Alpinion are leading companies in domestic ultrasound imaging industry. They have released many ultrasound imaging systems for OB/GYN, cardiology and radiology examinations. In this section, we deal with major imaging features contained in the ultrasound systems of Samsung Medison and Alpinion, and see how mathematics is related to the imaging features.

Based on the product information provided through the website or brochure, we compare the imaging technologies of WS80A with Elite and E-CUBE 15EX(Women's Health), which are high-performance imaging systems for OB/GYN application, of Samsung Medison and Alpinion, respectively. Table 1 shows most of imaging technologies are implemented by beamforming methods, signal processing, image processing methods such as speckle reduction, edge enhancement, contrast enhancement, edge detection and image segmentation, digital scan conversion and elasticity imaging methods. 3D volume rendering and visualization techniques are used very much, especially for OB/GYN applications. As we know already, these ultrasound imaging technologies are basically based on mathematical modelling, numerical solution and visualization.

Table 1. Comparison of imaging technologies of two domestic companies: Samsung Medison and Alpinion for OB/GYN ultrasound. (SCI: spatial compound imaging, FCI: frequency compound imaging, DSC: digital scan conversion)

Samsung Medison (WS80A with Elite)	Alpinion (E-CUBE 15EX)	Technologies
Features		
S-Harmonic	Harmonic Imaging	signal processing (filter design)
ClearVision™	Optimal Imaging Suite™	speckle reduction, edge enhancement, contrast enhancement, SCI, FCI
5D Heart Color (Fetal heart examination)	-	3D volume rendering, visualization
5D Limb Vol.	-	edge detection, automated measurement
5D CNS+ (Fetal brain measurement)	-	visualization, segmentation
5D NT (Nuchal translucency measurement)	Auto NT (Nuchal Translucency)	3D volume rendering, segmentation
5D Follicle (Follicle measurement)	-	3D visualization, segmentation
Realistic Vue™	Volume Master™, Live HQ™	3D volume rendering, 3D DSC
Crystal Vue	-	3D volume rendering, 3D DSC
ElastoScan™	Elastography	elasticity imaging
E-Breast™ (ElastoScan™ for Breast)		
E-Thyroid™ (ElastoScan™ for Thyroid)		
S-Detect	-	segmentation, edge detection
S-Vue Transducer	Crystal Signature™	transducer manufacture
Wide angle endocavity transducer (E3-12A, Max 210°)	Extreme High Density Endovaginal transducer (EV3-10X / EC3-10X, Max 230°)	beam-forming, DSC
-	Flow State	mathematical modelling, optimization
-	Auto Trace PW, CW	edge detection
-	Xpeed™	mathematical modelling, optimization

On the other hand, we compare the imaging features of two systems HS70A and E-CUBE 15EX(Cardiology) for cardiology application. Like in OB/GYN ultrasound, most of the imaging technologies shown in Table 2 are implemented by beam-forming methods, signal processing, image processing methods including cardiac wall motion tracking, digital scan conversion and elasticity imaging methods. Compared to OB/GYN ultrasound, two systems do not equip 3D volume rendering methods, but wall motion tracking methods. In order to develop accurate wall motion tracking methods, understanding and mathematical modelling of cardiac wall motion are indispensable for the technology advancements of cardiology ultrasound.

We note that Samsung Medison and Alpinion lack real-time 3D echocardiography in their released cardiac ultrasound imaging systems, as shown in Table 2. Real-time 3D echocardiography is related to beam-forming algorithms for 2D arrays, 3D rendering and visualization, 3D wall motion tracking methods, spatial/temporal resolution enhancement, and so on.

TABLE 2. Comparison of imaging technologies of two domestic companies: Samsung Medison and Alpinion for cardiology ultrasound.

Samsung Medison (HS70A)	Alpinion (E-CUBE 15EX)	
Features		Technologies
S-Harmonic	Advanced Harmonic Imaging	signal processing (filter design)
-	Anatomical M-mode	edge detection
-	Auto IMT	edge detection
Arterial Analysis (detection of functional changes of vessels)	-	edge detection, strain analysis
Strain+	CUBE Strain™	wall motion analysis, motion tracking
Stress Echo	Stress Echo	wall motion analysis, motion tracking
-	Echo Master™	measurement
-	Auto Trace PW, CW	edge detection
S-Detect™	-	segmentation, edge detection
E-Breast™	-	elasticity imaging
E-Thyroid™	-	elasticity imaging
S-Vue Transducer	high density single crystal phased array transducer	transducer manufacture
Advanced QuickScan™	Xpeed™	mathematical modelling, optimization

According to radiology applications, the imaging features of RS80A with Prestige and E-CUBE 15EX are listed in Table 3. Among the imaging features, S-Shearwave, S-Fusion and Respiration Auto are added imaging features for radiology ultrasound imaging. S-Shearwave computes the propagate velocity of the shearwave through the targeted lesion using elastic wave equation, while S-Fusion and Respiration Auto are based on image registration methods. S-Fusion enables simultaneous localization of a lesion with a real-time ultrasound in conjunction with other 3D volumetric imaging modalities. Unlike the conventional image fusion technology, Samsung offers a quicker and more precise registration process. Respiration Auto feature minimizes registration differences between the inhaled CT and exhaled ultrasound scan images by generating compensated exhaled CT image.

6. APPLICATION CASES OF MATHEMATICS

As shown in the previous sections, mathematics is widely used in ultrasound imaging. From the understanding of wave propagation and its scattering, beam-forming algorithms, digital

TABLE 3. Comparison of imaging technologies of two domestic companies: Samsung Medison and Alpinion for radiology ultrasound.

Samsung Medison (RS80A with Prestige)	Alpinion (E-CUBE 15EX)	Technologies
Features		
S-Harmonic	Harmonic Imaging	signal processing (filter design)
S-Vision beamformer	-	beam-forming
HQ Vision	SRI / FullSRI™	speckle reduction, edge enhancement, contrast enhancement, SRI, FCI
NeedleMate™	Needle Vision™	edge enhancement, contrast enhancement
CEUS+	-	contrast enhancement
S-Shearwave	-	elasticity imaging, elastic wave equation
S-Fusion	-	image registration
Respiration Auto	-	image registration
S-Tracking	-	edge detection
Arterial Analysis (detection of functional changes of vessels)	-	edge detection, strain analysis
S-3D Arterial Analysis (volume measurement of artery plaque)	-	segmentation, 3D visualization
Auto IMT+™	Auto IMT	edge detection
Strain+	-	wall motion analysis, motion tracking
Stress Echo	-	wall motion analysis, motion tracking
S-Detect™ for Breast, S-Detect™ for Thyroid	-	segmentation, edge detection
ElastoScan™	Elastography	elasticity imaging
E-Strain		
E-Breast™		
E-Thyroid™		
S-Vue Transducer	high density single crystal convex transducer, renowned ALPINION's linear transducer set	transducer manufacture
-	Panoramic Imaging	image registration
Advanced QuickScan™	Xpeed™	mathematical modelling, optimization

scan conversion, signal processing theory, various image processing methods, and so on. In this section, we introduce some practical cases of mathematical applications for ultrasound imaging: LV motion tracking problem, LV vortex flow imaging problem and elasticity imaging study. They were performed for an industry-university cooperation research, by the demands in healthcare or by the demands in ultrasound imaging industry.

6.1. **LV motion tracking problem.** We consider a problem on LV motion tracking and its solutions through mathematical models. The LV motion should be observed and analyzed for evaluations of ventricular systolic/diastolic function, subclinical disease including amyloidosis, LV hypertrophy and hypertrophic cardiomyopathy, coronary artery disease, and so on. Typically, LV motion tracking is performed by observing speckle pattern. Speckle is inherent appearance in ultrasound imaging and its local brightness reflects the local echogeneity of the underlying scatterers. We introduce a case of overcoming limitation in LV motion tracking problem.

6.1.1. *Commonly used LV tracking methods and their limitations.* Among various LV motion tracking methods such as deformable models, statistical methods, classification methods and so on, we can use optical flow methods. Optical flow methods are based on the assumption that

that the intensity of a moving object is constant over time. Let $I(\mathbf{r}, t)$ represent the intensity of echocardiography at the location $\mathbf{r} = (x, y)$ and the time t. Then the noisy time-varying images $I(\mathbf{r}, t)$ approximately satisfy

$$\mathbf{u}(\mathbf{r}, t) \cdot \nabla I(\mathbf{r}, t) + \frac{\partial}{\partial t} I(\mathbf{r}, t) \approx 0, \tag{6.1}$$

where $\mathbf{u}(\mathbf{r}, t)$ is the velocity or displacement vector to be estimated. Especially, Lucas and Kanade [48] used the locally constant motion to compute the velocity $\mathbf{u}(\mathbf{r}_0, t)$ at a target location $\mathbf{r}_0 = (x_0, y_0)$ and time t by forcing constant velocity in a local neighborhood of $\mathbf{r}_0 = (x_0, y_0)$ denoted by $\mathcal{N}(\mathbf{r}_0)$. Following them, Barron *et al.* [49] proposed an improved model to estimate the velocity $\mathbf{u}(\mathbf{r}_0, t)$ by minimizing the weighted least square criterion in the neighborhood $\mathcal{N}(\mathbf{r}_0)$:

$$\mathbf{u}(\mathbf{r}_0, t) := \arg\min_{\mathbf{u}} \int_{\mathcal{N}(\mathbf{r}_0)} \left[w(\mathbf{r} - \mathbf{r}_0) \left(\mathbf{u}(\mathbf{r}, t) \cdot \nabla I(\mathbf{r}, t) + \frac{\partial}{\partial t} I(\mathbf{r}, t) \right)^2 \right] d\mathbf{r}, \tag{6.2}$$

where w is a weight function.

On the other hand, region-based method (also known as the block matching or pattern matching method) can be also used as the LV motion tracking. Duan *et al.* [50] used the region-based method with cross-correlation coefficient as similarity measure as follows. For given two consecutive images $I(\cdot, t)$ and $I(\cdot, t + \Delta t)$, the displacement $\mathbf{u}(\mathbf{r}, t)$ at each position $\mathbf{r}$ and time t is estimated by maximizing the cross-correlation coefficient:

$$\mathbf{u}(\mathbf{r}_0, t) := \arg\max_{\mathbf{u}} \left\{ \frac{\int_{\mathcal{N}(\mathbf{r}_0)} [I(\mathbf{r}, t) I(\mathbf{r} + \mathbf{u}, t + \Delta t)] d\mathbf{r}}{\sqrt{\int_{\mathcal{N}(\mathbf{r}_0)} [I(\mathbf{r}, t)]^2 d\mathbf{r}} \sqrt{\int_{\mathcal{N}(\mathbf{r}_0)} [I(\mathbf{r} + \mathbf{u}, t + \Delta t)]^2 d\mathbf{r}}} \right\}. \tag{6.3}$$

However, there often exist some incorrectly tracked points in practical environment due to ultrasound artifacts, dropouts, or shadowing phenomena of cardiac wall [51]. It is problematic to track the LV border in ultrasound images with unclear speckle pattern or weak signals. In order to overcome this problems, Ahn [52] proposed a mathematical model for robust myocardial border tracking by considering an affine transformation to describe a global motion that is synthesized by integrating local deformations.

6.1.2. *A mathematical modelling for robust LV tracking.* We denote the LV border traced at initially selected frame by a parametric contour $\mathcal{C}^* = \{\mathbf{r}^*(s) = (x^*(s), y^*(s)) \mid 0 \le s \le 1\}$ that can be identified as its n tracking points $\mathbf{r}_1^* = \mathbf{r}^*(s_1), \cdots, \mathbf{r}_n^* = \mathbf{r}^*(s_n)$. Here, $0 = s_1 < s_2 < \cdots < s_n = 1$. Let $\mathcal{C}(t) = \{\mathbf{r}(s, t) = (x(s, t), y(s, t)) \mid 0 \le s \le 1\}$ be the contour deformed from $\mathcal{C}(0) = \mathcal{C}^*$ at time t. The motion of the contour $\mathcal{C}(t)$ will be determined by an appropriately chosen velocity $\mathbf{U}(t)$ indicating a time change of tracking points $(\mathbf{r}_1(t), \cdots, \mathbf{r}_n(t))$:

$$\mathbf{U}(t) := \begin{bmatrix} {}_1(t) \\ \vdots \\ {}_n(t) \end{bmatrix} = \frac{d}{dt} \begin{bmatrix} \mathbf{r}_1(t) \\ \vdots \\ \mathbf{r}_n(t) \end{bmatrix} \qquad \text{with} \qquad \begin{bmatrix} \mathbf{r}_1(0) \\ \vdots \\ \mathbf{r}_n(0) \end{bmatrix} = \begin{bmatrix} \mathbf{r}_1^* \\ \vdots \\ \mathbf{r}_n^* \end{bmatrix}$$

Here, we identify the contour $\mathcal{C}(t)$ with tracking points $(\mathbf{r}_1(t), \cdots, \mathbf{r}_n(t))$. We compute $\mathbf{U}(t)$ for each time t by minimizing the following energy functional reflecting local-to-global deformation:

$$\mathcal{E}_t(\mathbf{U}) := \frac{1}{2}\sum_{i=1}^{n}\left[\begin{array}{c} \int_{\mathcal{N}(\mathbf{r}_i(t))} w(\mathbf{r}' - \mathbf{r}_i(t))\left\{\mathbf{u}_i \cdot \nabla I(\mathbf{r}', t) + \frac{\partial}{\partial t} I(\mathbf{r}', t)\right\}^2 d\mathbf{r}' \\ +\lambda \left|\mathbf{r}_i(t) + \mathbf{u}_i - \begin{bmatrix} a_1(\mathbf{U}) & a_2(\mathbf{U}) \\ a_3(\mathbf{U}) & a_4(\mathbf{U}) \end{bmatrix} \mathbf{r}_i^* - \begin{bmatrix} a_5(\mathbf{U}) \\ a_6(\mathbf{U}) \end{bmatrix}\right|^2 \end{array}\right] \tag{6.4}$$

where λ is a nonnegative parameter and the affine coefficients $a_1(\mathbf{U}), \cdots, a_6(\mathbf{U})$ at time t are given by

$$\begin{bmatrix} a_1(\mathbf{U}) & a_3(\mathbf{U}) \\ a_2(\mathbf{U}) & a_4(\mathbf{U}) \\ a_5(\mathbf{U}) & a_6(\mathbf{U}) \end{bmatrix} = \left(\Phi(\mathcal{C}^*)^T \Phi(\mathcal{C}^*)\right)^{-1} \Phi(\mathcal{C}^*)^T \begin{bmatrix} (\mathbf{r}_1(t) + \mathbf{u}_1)^T \\ \vdots \\ (\mathbf{r}_n(t) + \mathbf{u}_n)^T \end{bmatrix}, \ \Phi(\mathcal{C}^*) := \begin{bmatrix} \mathbf{r}_1^{*T} & 1 \\ \vdots & \vdots \\ \mathbf{r}_n^{*T} & 1 \end{bmatrix}.$$

This study has been performed as an industry-university cooperation research. Based on the proposed model, LV tracking methods of improved performance are being developed.

6.2. **A new imaging mode: vortex flow imaging.** Vortex flow imaging has recently attracted much attention as a new application for evaluating blood flow [53–55], because it visualizes and quantifies time-varying blood flow inside LV using available ultrasound data. It has shown the potential possibility and availability for evaluating blood flow. In order to compute the velocity fields of blood flow, it is required to model blood flow based on fluid equation.

6.2.1. *A reconstruction problem of blood flow.* With echo-PIV(particle image velocimetry) [56, 57] being representative, there are several methods to compute and visualize the velocity fields of blood flow inside LV. Echo-PIV is based on optical flow methods tracking the speckle patterns of blood flow to estimate blood motion. However, Echo-PIV is not completely noninvasive because it requires the intravenous injection of a contrast agent to obtain images suitable for the speckle tracking algorithm. To develop less invasive techniques, methods to reconstruct blood flows from color Doppler images have been proposed [58–63]. We represent mathematical models to reconstruct the velocity of blood flow, especially using color Doppler data reflecting one-directional velocity components of blood flow along scanlines.

6.2.2. *A mathematical modelling of 3D blood flow.* Let D be a 3D imaging domain, $\Omega(t)$ a time-varying LV region satisfying $\Omega(t) \subseteq D \subseteq \mathbb{R}^3$, and T a beat cycle. For the beat cycle T, we consider a spatial-temporal domain Ω_T defined by $\Omega_T := \bigcup_{0<t<T} \Omega(t) \times \{t\} \subseteq D \times (0, T)$. Let $\mathbf{v}(\mathbf{r}, t)$ be a velocity field of the blood flow in $\Omega_t \in \Omega_T$ at time t. Then the fluid equations governing the blood flow $\mathbf{v}$ is given by the 3D incompressible Navier-Stokes equations:

$$\begin{cases} \tilde{\rho}\left(\dfrac{\partial \mathbf{v}}{\partial t} + \mathbf{v} \cdot \nabla \mathbf{v}\right) = -\nabla p + \tilde{\mu}\nabla^2 \mathbf{v} & \text{in } \Omega_t, \\ \nabla \cdot \mathbf{v} = 0 & \text{in } \Omega_t. \end{cases} \tag{6.5}$$

In order to solve (6.5), we need proper boundary conditions or some conditions based on ultrasound measurement data as follows:

Let $\mathbf{a}(\mathbf{r})$ be scanline directional unit vector at the position $\mathbf{r} \in D$ and $\mathcal{D}(\mathbf{r}, t)$ color Doppler image in Ω_t. Given $\mathcal{D}(\mathbf{r}, t)$, we then consider an inverse problem to find a 3D vector field $\mathbf{v} = (u, v, w)$ satisfying the following condition:

$$\mathbf{a}(\mathbf{r}) \cdot \mathbf{v}(\mathbf{r}, t) = \mathcal{D}(\mathbf{r}, t). \tag{6.6}$$

However, in clinical practice, it is currently very difficult to acquire 3D color Doppler images given by (6.6). A mathematical model appropriate to the measurements on 2D ultrasound imaging should be considered.

6.2.3. *A reconstruction model with mass-source term.* Jang *et al.* [64] suggested a 2D reconstruction model using incompressible Navier-Stokes equations with mass-source term s to reflect 3D motion of blood flow as the following: Let D be a 2D imaging domain and $\Omega(t)$ the cross-section of the LV region in the A3CH view so that they satisfy $\Omega(t) \subseteq D \subseteq \mathbb{R}^2$ and $\mathbf{v}(\mathbf{x}, t) = (u(\mathbf{x}, t), v(\mathbf{x}, t))$ the velocity fields of flow at the position $\mathbf{x} \in D$ and time t. Then the fluid equations governing the blood flow on the imaging plane D are modeled as

$$\begin{cases} \dfrac{\partial u}{\partial t} + u\dfrac{\partial u}{\partial x} + v\dfrac{\partial u}{\partial y} = -\dfrac{1}{\tilde{\rho}}\dfrac{\partial p}{\partial x} + \dfrac{\tilde{\mu}}{\tilde{\rho}}\nabla^2 u + \dfrac{\tilde{\mu}}{3\tilde{\rho}^2}\dfrac{\partial s}{\partial x}, \\ \dfrac{\partial v}{\partial t} + u\dfrac{\partial v}{\partial x} + v\dfrac{\partial v}{\partial y} = -\dfrac{1}{\tilde{\rho}}\dfrac{\partial p}{\partial y} + \dfrac{\tilde{\mu}}{\tilde{\rho}}\nabla^2 v + \dfrac{\tilde{\mu}}{3\tilde{\rho}^2}\dfrac{\partial s}{\partial y}, \\ \dfrac{\partial u}{\partial x} + \dfrac{\partial v}{\partial y} = \dfrac{s}{\tilde{\rho}}, \end{cases} \tag{6.7}$$

We note that this model (6.7) is equivalent to a 2D incompressible flow having a source-sink distribution $s(\mathbf{x}, t)$ [65]. In order to solve (6.7), we consider color Doppler images measured practically in the imaging plane D. We set the 3D coordinate system for the xy-plane to contain $\Omega(t)$ and the z-axis to be normal to this plane. Let $\mathcal{D}(\mathbf{x}, t)$ be the measured color Doppler data, expressed as the inner product of the scanline vector and the velocity vector

$$\mathcal{D}(\mathbf{x}, t) = (a_1(\mathbf{x}), a_2(\mathbf{x})) \cdot (u(\mathbf{x}, t), v(\mathbf{x}, t)). \tag{6.8}$$

Therefore, we obtain a mathematical problem to find $\mathbf{v}$ satisfying (6.7) and (6.8) simultaneously. Some numerical simulations are performed for solving the given problem and validating the proposed mathematical model.

6.3. **Acoustic radiation force-based elastography.** Acoustic radiation force(ARF) is caused by absorbed ultrasound wave energy while ultrasound wave propagates through soft tissues. The absorbed energy accumulates in tissue and it generates volume force in the propagation direction of ultrasound beam. This ARF technique enables inducing stress at desired position and measuring response to the stress with a single ultrasound system, whereas other elastography techniques require manual push or additional devices to induce stress or shear waves [66]. We consider ARF-based shear wave elasticity imaging (SWEI) that maps tissue elasticity by

measuring the propagation speed of shear waves generated by ARF. The propagation speed c is expressed as

$$c = \sqrt{\frac{\mu}{\rho}},$$

where μ and ρ are the shear modulus and density of tissue, respectively. We note that tissue elasticity can be quantified by estimating c.

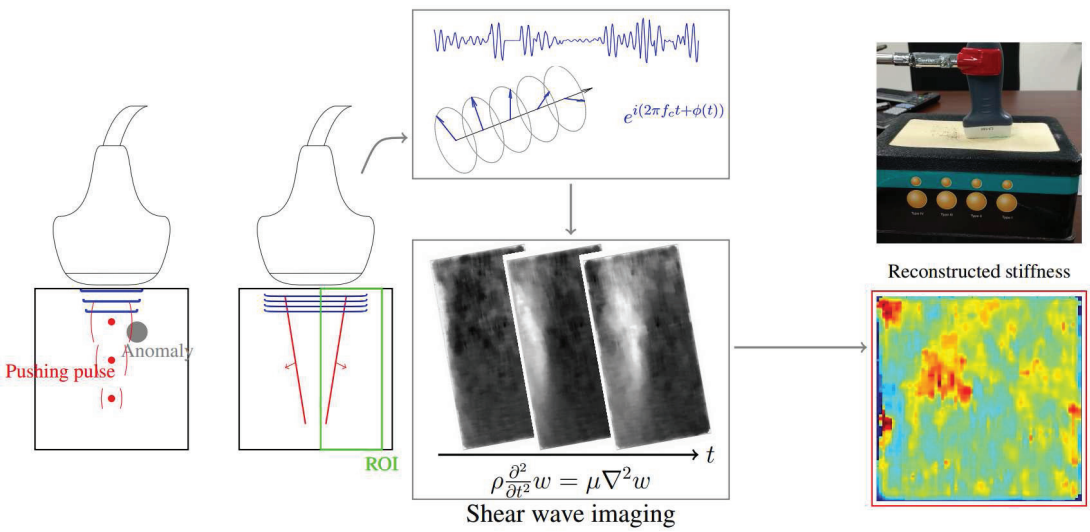

FIGURE 5. A description of elasticity imaging using shear wave. The propagation of shear wave is observed through ultrasound images, acquired from a research ultrasound system E-CUBE 12R (Alpinion, Korea).

6.3.1. *Mathematical model.* An inverse problem for ARF-based ultrasound elastography is to reconstruct the shear modulus μ from the measured axial movement w which satisfies

$$\rho\frac{\partial^2 w}{\partial t^2} = \mu\nabla^2 w + f_z \quad \text{in } \mathbb{R}^3 \times (0,T), \tag{6.9}$$

where f_z is induced ARF in the axial direction, that is, the vertical direction in imaging planes shown in Fig. 5. Note that the excitation f_z and the induced displacement w are not time-harmonic. Let $\text{supp}(f_z)$ be the support of f_z in the spatio-temporal domain. Then, we assume that $\text{supp}(f_z)$ is given because it is possible to change a focal point for inducing ARF. Moreover, we assume that $f_z = 0$ out of $\text{supp}(f_z)$ to avoid the difficulty in quantifying f_z due to the uncertainty of medium [67]. Then, the inverse problem is formulated as a problem to reconstruct the shear modulus μ from the measured axial movement w satisfying

$$\rho\frac{\partial^2 w}{\partial t^2} = \mu\nabla^2 w \quad \text{in } (\mathbb{R}^3 \times (0,T)) \setminus \text{supp}(f_z). \tag{6.10}$$

Nightingale *et al.* [68] suggested the algebraic inversion of the equation in (6.10) to estimate $\frac{\mu}{\rho}$:

$$\frac{\mu}{\rho} = \frac{\frac{\partial^2 w}{\partial t^2}}{\nabla^2 w} \tag{6.11}$$

However, it could be unstable since numerical approximation of second-order derivatives in (6.10) are sensitive to noise. In many approaches, wave propagation speed is estimated by computing $\frac{\mu}{\rho}$ instead of the direct inversion [46, 47, 69].

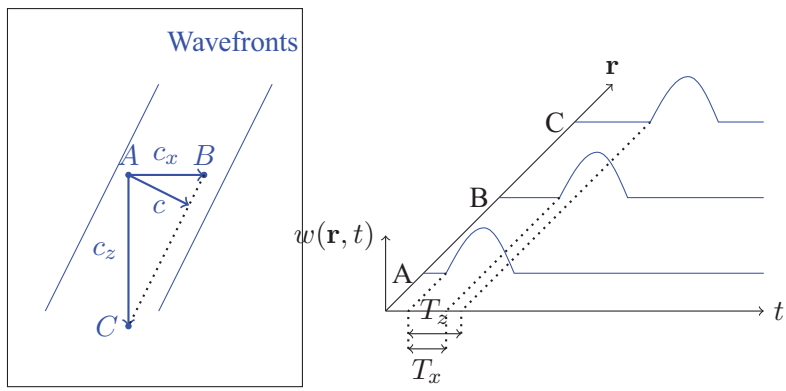

$$c = \frac{c_x c_z}{\sqrt{c_x^2 + c_z^2}} \qquad c_x = \frac{|\mathbf{r}_A - \mathbf{r}_B|}{T_x} \quad c_z = \frac{|\mathbf{r}_A - \mathbf{r}_C|}{T_z}$$

FIGURE 6. Illustration of time delays T_x and T_z for estimating the lateral speed c_x and axial speed c_z of shear wave propagation.

We consider time delay to estimate the shear wave propagation speed. As shown in Fig. 6, let T_x be the time delay, that is, the difference between arrival times of the displacement signal by shear wave propagation at two positions A and B placed on a lateral line. Then the shear wave propagation speed c_x in the lateral direction is given by

$$c_x = \frac{|\mathbf{r}_A - \mathbf{r}_B|}{T_x}, \tag{6.12}$$

where $\mathbf{r}_A$ and $\mathbf{r}_B$ are the coordinates of A and B, respectively. Therefore, T_x is computed by

$$T_x = \arg\max_{\tau \in (0,T)} \int_0^T w(x_1, t) w(x_2, t - \tau) dt. \tag{6.13}$$

Since the wave propagation direction may not be parallel to the lateral direction (Fig. 6) in many cases of ARF-based excitation, we deal with the shear wave propagation speed c_z in the axial direction. Likewise, let T_z be the time delay, that is, the difference between arrival times

of the displacement signal by shear wave propagation at two positions A and C placed on a axial line. Then c_z is expressed as

$$c_z = \frac{|\mathbf{r}_A - \mathbf{r}_C|}{T_z}, \tag{6.14}$$

where $\mathbf{r}_C$ is the coordinate of C. From c_x and c_z, we can compute the propagation speed velocity c [70]:

$$c = \frac{c_x c_y}{\sqrt{c_x^2 + c_z^2}}. \tag{6.15}$$

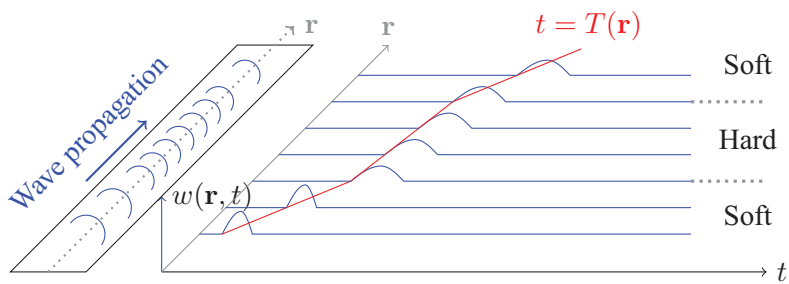

FIGURE 7. A simple description of TOF approach. The disturbance of blue curve corresponds to the displacement at offset from the source. Arrival time of the wave-front is tracked by the red line.

6.3.2. *Eikonal equation-based approaches.* As illustrated in Fig. 7, wave propagation speed can be estimated from the slope between offset position and arrival time of wave-front. The propagation speed c can be estimated by the gradient of arrival time T using the Eikonal equation [71]:

$$|\nabla T| = \frac{1}{c}, \tag{6.16}$$

where $T(\mathbf{r})$ is defined by

$$T(\mathbf{r}) = \inf\{t > 0 : |w(\mathbf{r}, t)| > 0\}. \tag{6.17}$$

In a realistic case, $T(\mathbf{r})$ is estimated by using a fixed threshold δ above a noise level of the estimated $w(\mathbf{r}, t)$ [72]:

$$T(\mathbf{r}) \approx \inf\{t > 0 : |w(\mathbf{r}, t)| > \delta\}. \tag{6.18}$$

As an alternative way, the biased cross-correlation C is suggested by McLaughlin *et al.* [73]

$$T(\mathbf{r}) \approx \arg\max_{\tau \in (0,T)} \frac{1}{T} \int_0^T w(\mathbf{r}_{\text{ref}}, t)\tilde{w}(\mathbf{r}, t - \tau)dt \quad \text{for } \mathbf{r}_{\text{ref}} \text{ a reference point,} \tag{6.19}$$

where

$$\tilde{w}(\mathbf{r},t) = \begin{cases} w(\mathbf{r},t) & \text{if } 0 \le t \le T, \\ w(\mathbf{r},t-T) & \text{if } t \ge T, \\ w(\mathbf{r},t+T) & \text{if } t \le 0. \end{cases} \tag{6.20}$$

7. Current Hot Topics and Challenging Issues

In this section, we introduce current hot topics in ultrasound imaging, especially in the domestic ultrasound industry. Samsung Medison, a global medical equipment company and a leading domestic company, has recently published some white papers [74–80] on: S-Detect™, 5D CNS, E-Thyroid™, E-Breast™(breast ElastoScan™), S-Shearwave, Aterial Analysis, and so on. The white papers report the advantages and shortcomings of each technology.

7.1. **Hot topics in ultrasound imaging.**

- S-Detect™ is a software analyzing the features of lesions and assessing the possibility of malignancy. It uses a machine learning-based algorithm [81]. By showing excellent agreement of 91.2% with the assessment of breast dedicated radiologist in interpreting the breast mass, it is suggested as a good decision-making support for the beginners or non-breast radiologists. However, with the sensitivity of 84.6% at the same time, it missed two breast cancers of relatively circumscribed isoechoic and hypoechoic masses with suspicious clinical findings. Therefore, it is reported that circumscribed malignant masses may be remained as the limitation of S-Detect™ and S-Detect™ is not available to find subtle suspicious features [74].
- A semi-automatic method is proposed for biometric measurements of fetal central nervous system(CNS) from 3D ultrasound volume data of brain. It reduce the number of operations and examination time. Its high success rate $>90\%$ is reported under clinical evaluation [75].
- E-Thyroid™ uses carotid artery pulsation, not external compression by free hands, as a compression source. While E-Thyroid™ effectively differentiates malignant from benign in most thyroid nodules including calcified nodule, the extreme location of a nodule in the tyroid can affect the results [76].
- E-Breast™ is helpful for characterizing different regions as a complementary diagnostic imaging technology, based on strain imaging technique. However, it would be important not to evaluate a lesion from an isolated manner with strain ratio generated from E-Breast™ [77].
- S-Shearwave is a technology enabling quantitative analysis of tissue stiffness for assessing liver fibrosis. Unlike the color map used in the conventional elasticity imaging, S-Shearwave displays the stiffness value and Reliable Measurement Index(RMI) for the region of interest [78].

Among them, S-Detect™, 5D CNS and Aterial Analysis are CADe/CADx softwares. There are numerous demands of CADe and CADx for many medical imaging methodologies [82–85] as well as ultrasound [86–88]. According to the applications, CADe is implemented by various

image processing methods: histogram-based thresholding and active contours for segmenting anomaly [83], neural network-based approaches for robust segmentation [89–91]. In the literatures [86, 87], it is reported that neural network and support vector machine techniques are used for CADx.

On the other hand, currently commercialized elasticity imaging modes:E-Thyroid™, E-Breast™, S-Shearwave [76–78] are commonly used as a complementary diagnostic tool. It is required to quantify more accurately the stiffness of tissues.

Fusion imaging techniques have been used for volume navigation of 2D ultrasound images within other 3D CT or MR images. In order to register different images acquired from medical imaging modalities, the fusion imaging techniques have been developed with the help of landmarks, position sensors, or electromagnetic needle tracking [92–94]. As real-time 3D ultrasound imaging becomes feasible, fusion imaging technique for 3D volume data is considered as a promising tool for computer-aided surgery [94–96]. In 3D fusion imaging, external devices such as landmarks, position sensors or electromagnetic needle tracking can be removed [97,98]. Samsung Medison developed the fusion imaging techniques called S-Fusion.

Additionally, we introduce some issues in ultrasound imaging, related to mathematical modelling, numerical solutions, image processing and visualization.

7.2. **Issues on LV tracking methods.**

- Real-time 3D ultrasound imaging is capable of providing good 3D visualization of organs. However, its resolution is not good enough to discriminate features smaller than a few millimeters and LV tracking methods based on speckles are not appropriate to be applied to 3D ultrasound images. We can consider 3D LV tracking by constructing the motion of 3D LV shape from 2D LV borders, which are extracted by applying LV tracking methods to multiple 2D echocardiography data. How can we model the relationship between the change of LV borders observed on 2D echocardiography and the 3D LV shape?
- LV motion tracking methods include inevitable limitation on 2D echocardiography because of the helical structure of cardiac ventricular anatomy. For a heartbeat cycle, it is difficult to track a portion of LV border designated at the initial stage on a 2D ultrasound image. In fact, it gets out of the imaging plane. How can we model the relationship between the change of LV borders observed on 2D echocardiography and the 3D helical behavior of cardiac motion?

7.3. **Issues on vortex flow imging.**

- Vortex flow imaging consists of defining LV geometry from echocardiographic images and reconstructing the velocity field of blood flow in the moving LV region. Let us assume that the acquisition of 3D color Doppler imaging at high frame rate is available. Can we model an inverse problem for reconstructing the 3D velocity field of blood flow from the partial velocity information obtained through the 3D color Doppler images? [99].

7.4. **Issues on elasticity imaging.**

- Inherent low SNR of the estimated w makes the direct inversion (6.11) difficult so that many models reconstructing c are based on the time-of-flight(TOF)-based approaches. However, they do not fully guarantee stability in practical situations since the inverse of time-delay or $|\nabla T|$ are still necessary for the speed estimation. In order to overcome the problem, Wang *et al.* suggest a fitting model for the estimated $T(\mathbf{r})$ [100]

$$T(\mathbf{r}) = \boldsymbol{\beta} \cdot \mathbf{r} + t_0, \tag{7.1}$$

where t_0 is a fitting parameter and $\boldsymbol{\beta}$ a fitting parameter vector satisfying

$$|\boldsymbol{\beta}| = c. \tag{7.2}$$

However, in inhomogeneous medium, the fitting model (7.1) could not describe $T(\mathbf{r})$ properly because refraction on the boundary between different tissues makes non-linear distortion of arrival-time. We need a modified fitting model for $T(\mathbf{r})$ which assumes the presence of anomaly.

8. Conclusion

Ultrasound imaging industry is very promising in terms of technology advancements as well as the market size and growth. Like in other industries, the ultrasound imaging technologies have been advanced and innovated through *Mathematics*. In this article, we described the history of ultrasound imaging, its basic principle, its diagnostic applications, domestic-industrial products, practical use of mathematics, hot topics and challenging issues related to ultrasound imaging. Through them, we confirmed that *Mathematics* has been used commonly as mathematical modelling, numerical solutions and visualization, combined with science, engineering and medicine in ultrasound imaging.

The practical use of *Mathematics* in ultrasound imaging requires the understanding of human body and imaging system overall. Based on that understanding, we should perform physics-based mathematical modelling, deal with the measurement data acquired through ultrasound imaging systems and solve various problems and challenging issues in ultrasound imaging.

Currently, there are still numerous demands of technology advancements in healthcare and ultrasound imaging industry, especially in domestic ultrasound industry. As we have seen before, *Mathematics* can contribute to the advances and innovation of ultrasound imaging technology. We hope many mathematicians contribute much to ultrasound technology innovation.

Acknowledgements

This work was supported by the National Institute for Mathematical Sciences(NIMS) and the National Research Foundation of Korea (NRF) grants funded by the Korea government(No. NRF-20151009350). We would like to thank reviewers for their detailed comments and suggestions to improve the paper. Also, we thank Haeeun Han for her help with rendering the TOC art.

REFERENCES

[1] Medical Equipment Market Size & Growth - Diagnostic Imaging[Ultrasound Systems] Market, *Global 2006-2013, USD Constant Millions, Global Data*, https://medical.globaldata.com.

[2] Medical Equipment Market Size & Growth - Diagnostic Imaging[Ultrasound Systems] Market, *Global 2013-2020, USD Constant Millions, Global Data*, https://medical.globaldata.com.

[3] Medical Equipment Market Size & Growth - Diagnostic Imaging[Ultrasound Systems] Company Shaare By Percentage, *Global 2012, USD Constant Millions, Global Data*, https://medical.globaldata.com.

[4] T. Szabo, *Diagnostic Ultrasound Imaging: Inside Out*, Academic Press, Boston University, 2004.

[5] D. H. Evans and W. N. McDicken, *Doppler Ultrasound - Physics, Instrumentation and Signal Processing, 2nd ed.*, John Wiley and Sons, New York, 2000.

[6] J. Woo, *A short history of the developments of ultrasound in obstetrics and gynecology.* http://www.ob-ultrasound.net/hydrophone.html, 1999.

[7] A.M. King, *Development, advances and applications of diagnostic ultrasound in animals*, The Veterinary Journal, **171**3 (2006), 408–420.

[8] J. Curie and P. Curie, *Development par pression de l'ectricite polaire dans les cristaux hemidres a faces inclinees*, Compte Rendue de l' Acadamie Scientifique, **91** (1880), 294–295.

[9] K. T. Dussik, *Über die Möglichkeit, hochfrequente mechanische Schwingungen als diagnostisches Hilfsmittel zu verwerten*, Zeitschrift für die gesamte Neurologie und Psychiatrie, **174**(1) (1942), 153–168.

[10] G. D. Ludwig and F. W. Struthers, *Considerations underlying the use of ultrasound to detect gall stones and foreign bodies in the tissues*, United States Navy Medical Research Institute Report, **4** (1949), 1–27.

[11] I. Donald, J. Macvicar and T. G. Brown, *Investigation of abdominal masses by pulsed ultrasound*, Lancet, **1** (1958), 1189–1195.

[12] Y. Nimura, *History of pulse and echo Doppler ultrasound in Japan*, Cardiac Doppler Diagnosis, Martimus Nijoff Publishers, Boston, 1983.

[13] R. W. J. Felix, B. Sigel, R. J. Gibson, J. Williams and G. L. Popky, *Pulsed Doppler ultrasound detection of flow disturbances in arteriosclerosis*, J. Clin. Ultrasound, **4**(4) (1976), 275–282.

[14] D. S. Evans and F. B. Cockett, *Diagnosis of deep-vein thrombosis with an ultrasonic Doppler technique*, Br. Med. J., **2** (1969), 802–804.

[15] P. N. T. Wells, *A range-gated ultrasonic Doppler system*, Medical and Biological Engineering, **7**(6) (1969), 641–652.

[16] G. R. Curry and D. N. White, *Color coded ultrasonic differential velocity arterial scanner (Echoflow)*, Ultrasound Med. Biol., **4** (1978), 27–35.

[17] B. Sigel, *A brief history of Doppler ultrasound in the diagnosis of peripheral vascular disease*, Ultrasound Med. Biol., **24**(2) (1998), 169–176.

[18] J. F. Brinkley, S. K. Muramatsu, W. D. McCallum and R. L. Popp, *In vitro evaluation of an ultrasonic three-dimensional imaging and volume system*, Ultrasonic Imaging, **4**(2) (1982), 126–139.

[19] K. Baba, K. Satoh, S. Sakamoto, T. Okai and S. Ishii, *Development of an ultrasonic system for three-dimensional reconstruction of the fetus*, Journal of Perinatal Medicine-Official Journal of the WAPM, **17**(1) (1989), 19–24.

[20] J. Deng, J. E. Gardener, C. H. Rodeck and W. R. Lees, *Fetal echocardiography in three and four dimensions*, Ultrasound Med. Biol., **22**(8) (1996), 979–986.

[21] S. L. Kobal, S. S. Lee, R. Willner, F. E. A. Vargas, H. Luo, C. Watanabe, Y. Neuman, T. Miyamoto and R. J. Siegel, *Hand-carried cardiac ultrasound enhances healthcare delivery in developing countries*, Am. J. Cardiol., **94**(4) (2004), 539-541.

[22] H. Shmueli, Y. Burstein, I. Sagy, Z. H. Perry, R. Ilia, Y. Henkin, T. Shafat, N. Liel-Cohen and S. L. Kobal, *Briefly Trained Medical Students Can Effectively Identify Rheumatic Mitral Valve Injury Using a Hand?Carried Ultrasound*, Echocardiography, **30**(6) (2013), 621–626.

[23] J. S. Shanewise, A. T. Cheung, S. Aronson, W. J. Stewart, R. L. Weiss, J. B. Mark, R. M. Savage, P. Sears-Rogan, J. P. Mathew, M. A. Quiñones, M. K. Cahalan MK and J. S. Savino, *ASE/SCA guidelines for performing a comprehensive intraoperative multiplane transesophageal echocardiography examination: recommendations of the American Society of Echocardiography Council for Intraoperative Echocardiography and the Society of Cardiovascular Anesthesiologists Task Force for Certification in Perioperative Transesophageal Echocardiography*, Anesth. Analg., **89**(4) (1999), 870–884.

[24] H. F. Andersen, *Transvaginal and transabdominal ultrasonography of the uterine cervix during pregnancy*, Journal of Clinical Ultrasound, **19**(2) (1991), 77–83.

[25] J. A. Jensen, D. Gandhi and W. D. O'Brien, *Ultrasound fields in an attenuating medium*, Proceedings of the IEEE 1993 Ultrasonics Symposium, 1993.

[26] A. Macovski, *Ultrasonic imaging using arrays*, Proceedings of the IEEE, 1979.

[27] J. A. Jensen, *A Model for the Propagation and Scattering of Ultrasound in Tissue*, J. Acoust. Soc. Am., **89** (1991), 182–191.

[28] J. A. Jensen and N. B. Svendsen, *Calculation of pressure fields from arbitrarily shaped, apodized, and excited ultrasound transducers*, IEEE Trans. Ultrason., Ferroelec., Freq. Contr., **39** (1992), 262–267.

[29] J. A. Jensen, *Field: A Program for Simulating Ultrasound Systems*, the 10th Nordic-Baltic Conference on Biomedical Imaging Published in Medical & Biological Engineering & Computing, **34** (1996), 351–353.

[30] AIUM, *AIUM Practice Parameter for the Performance of Obstetric Ultrasound Examinations*, http://www.aium.org/resources/guidelines/obstetric.pdf, 2013.

[31] R. Rastogi, G. L. Meena, N. Rastogi and V. Rastogi, *Interstitial ectopic pregnancy: A rare and difficult clinicosonographic diagnosis*, J. Hum. Reprod. Sci., **1**(2) (2008), 81–82.

[32] L. F. Gonçalves, W. Lee, J. Espinoza and R. Romero,*Three-and 4-Dimensional Ultrasound in Obstetric Practice Does It Help?*, J. Ultrasound Med., **24**(12) (2005), 1599–1624.

[33] N. J. Dudley, *A systematic review of the ultrasound estimation of fetal weight*, Ultrasound Obstet. Gynecol., **25**(1) (2005), 80–89.

[34] S. Feng, K. S. Zhou and W. Lee, *Automatic fetal weight estimation using 3D ultrasonography*, Proceedings of Medical Imaging 2012: Computer-Aided Diagnosis, California, USA 2012.

[35] I.-W. Lee, C.-H. Chang, Y.-C. Cheng, H.-C. Ko and F.-M. Chang, *A review of three-dimensional ultrasound applications in fetal growth restriction*, Journal of Medical Ultrasound, **20**(3) (2012), 142–149.

[36] S. Yagel, S. M. Cohen, I. Shapiro and D. V. Valsky, *3D and 4D ultrasound in fetal cardiac scanning: a new look at the fetal heart*, Ultrasound Obstet. Gynecol., **29**(1) (2007), 81–95.

[37] B. Messing, S. M. Cohen, D. V. Valsky, D. Rosenak, D. Hochner-Celnikier, S. Savchev and S. Yagel, *Fetal cardiac ventricle volumetry in the second half of gestation assessed by 4D ultrasound using STIC combined with inversion mode*, Ultrasound Obstet. Gynecol., **30**(2) (2007), 142–151.

[38] H. Laurichesse–Delmas, O. Grimaud, G. Moscoso and Y. Ville, *Color Doppler study of the venous circulation in the fetal brain and hemodynamic study of the cerebral transverse sinus*, Ultrasound in Obstetrics and Gynecology, **13**(1) (1999), 34–42.

[39] R. K. Pooh and K. Pooh, K,. *Transvaginal 3D and Doppler ultrasonography of the fetal brain*, Seminars in perinatology 2001, **25**(1) (2001), 38–43.

[40] W. Sepulveda, I. Rojas, J. A. Robert, C. Schnapp and J. L. Alcalde, *Prenatal detection of velamentous insertion of the umbilical cord: a prospective color Doppler ultrasound study*, Ultrasound in obstetrics & gynecology, **21**(6) (2003), 564–569.

[41] D. E. Fitzgerald and J. E. Drumm, *Non-invasive measurement of human fetal circulation using ultrasound: a new method*, Br. Med. J., **2**(6100) (1977), 1450–1451.

[42] A. Dall'Asta, G. Paramasivam, C. C. Lees, *Crystal Vue technique for imaging fetal spine and ribs*, Ultrasound in Obstetrics & Gynecology , **47**(3) (2016), 383–384.

[43] T. Reynolds, *The Echocardiographer's Pocket Reference, 4th Edition*, Arizona Heart Institute, Phoenix, Arizona, USA, 2013.

[44] E. G. Grant, C. B. Benson, G. L. Moneta, A. V. Alexandrov *et al.*, *Carotid artery stenosis: gray-scale and Doppler US diagnosis–Society of Radiologists in Ultrasound Consensus Conference*, Radiology, **229**(2) (2003), 340–346.

[45] A. T. Stavros, D. Thickman, C. L. Rapp, M. A. Dennis, S. H. Parker and G. A. Sisney, *Solid breast nodules: use of sonography to distinguish between benign and malignant lesions*, Radiology, **196**(1) (1995), 123–134.

[46] M. L. Palmeri, M. H. Wang, J. J. Dahl, K. D. Frinkley and K. R. Nightingale, *Quantifying hepatic shear modulus in vivo using acoustic radiation force*, Ultrasound in Medicine & Biology, **34**(4) (2008), 546–558.

[47] M. Tanter, J. Bercoff, A. Athanasiou, T. Deffieux, J.-L. Gennisson, G. Montaldo, M. Muller, A. Tardivon and M. Fink, *Quantitative assessment of breast lesion viscoelasticity: initial clinical results using supersonic shear imaging*, Ultrasound in Medicine & Biology, **34**(9) (2008), 1373–1386.

[48] B. Lucas, T. Kanade, *An iterative image restoration technique with an application to stereo vision*, Proceedings of DARPA IU Workshop, (1981), 121–130.

[49] J. L. Barron, D. J. Fleet, S. S. Beauchemin, *Performance of optical flow techniques*, Int. J. Comput. Vision, **12**(1) (1994), 43–77.

[50] Q. Duan, E. D. Angelini, S. L. Herz, C. M. Ingrassia, K. D. Costa, J. W. Holmes, S. Homma and A. F. Laine, *Region-Based Endocardium Tracking on Real-Time Three-Dimensional Ultrasound*, Ultrasound Med. Biol., **35**(2) (2009), 256–265.

[51] K. Y. E. Leung, M. G. Danilouchkine, M. van Stralen, N. de Jong, A. F. van der Steen and J. G. Bosch, *Left ventricular border tracking using cardiac motion models and optical flow*, Ultrasound Med. Biol., **37**(4) (2011), 605–616.

[52] C. Y. Ahn, *Robust Myocardial Motion Tracking for Echocardiography: Variational Framework Integrating Local-to-Global Deformation*, Computational and Mathematical Methods in Medicine, **2013** (2013), 974027.

[53] G.-R. Hong, G. Pedrizzetti, G. Tonti, P. Li, Z. Wei, J. K. Kim, A. Baweja, S. Liu, N. Chung, H. Houle, J. Narula, and M. A. Vannan, *Characterization and Quantification of Vortex Flow in the Human Left Ventricle by Contrast Echocardiography Using Vector Particle Image Velocimetry*, JACC: Cardiovascular Imaging, **1**(6) (2008), 705-717.

[54] P. P. Sengupta, G. Pedrizzetti, P. J. Kilner, A. Kheradvar, T. Ebbers, G. Tonti, A. G. Fraser and J. Narula, *Emerging Trends in CV Flow Visualization*, JACC: Cardiovascular Imaging, **5**(3) (2012), 305-316.

[55] D. R. Muñoz, M. Markl, J. L. Moya Mur, A. Barker, C. Fernández-Golfin, P. Lancellotti and J. L. Z. Gómez, *Intracardiac flow visualization: current status and future directions*, European Heart Journal- Cardiovascular Imaging, **14** (2013), 1029-1038.

[56] H. Gao, P. Claus, M.-S. Amzulescu, I. Stankovic, J. D'Hooge and J.-U. Voigt, *How to optimize intracardiac blood flow tracking by echocardiographic particle image velocimetry? Exploring the influence of data acquisition using computer-generated data sets*, European Heart Journal Cardiovascular Imaging, **13**(6) (2012), 490-499.

[57] H. Gao, B. Heyde and J. D'Hooge, *3D Intra-cardiac flow estimation using speckle tracking: a feasibility study in synthetic ultrasound data*, Proceedings of the IEEE International Ultrasonics Symposium (IUS'13), Prague, Czech Republic, July 2013.

[58] D. Garcia, J. C. Del Álamo, D. Tanné, R. Yotti, C. Cortina, É. Bertrand, J. C. Antoranz, E. Pérez-David, R. Rieu, F. Fernández-Avilés and others, *Two-dimensional intraventricular flow mapping by digital processing conventional color-doppler echocardiography images,* IEEE Transactions on Medical Imaging, **29**(10) (2010), 1701–1713.

[59] S. Ohtsuki and M. Tanaka, *The flow velocity distribution from the Doppler information on a plane in three-Dimensional flow,* Journal of Visualization, **9**(1) (2006), 69–82.

[60] M. Arigovindan, M. Suhling, C. Jansen, P. Hunziker and M. Unser, *Full motion and flow field recovery from echo Doppler data,* IEEE Transactions on Medical Imaging, **26**(1) (2007), 31–45.

[61] A. Gomez, K. Pushparajah, J. M. Simpson, D. Giese, T. Schaeffter and G. Penney, *A sensitivity analysis on 3D velocity reconstruction from multiple registered echo Doppler views,* Medical Image Analysis, **17**(6) (2013), 616–631.

[62] A. Gomez, A. de Vecchi, M. Jantsch, W. Shi, K. Pushparajah, J. M. Simpson, N. P. Smith, D. Rueckert, T. Schaeffter and G. P. Penney, *4D blood flow reconstruction over the entire ventricle from wall motion and blood velocity derived from ultrasound data,* IEEE Trans. on Medical Imaging, **34**(11) (2015), 2298–2308.

[63] F. Mehregan, F. Tournoux, S. Muth, Pibarot, Philippe and R. Rieu, G. Cloutier and D. Garcia, *Doppler vortography: a color doppler approach to quantification of intraventricular blood flow vortices,* Ultrasound in Medicine and Biology, **40**(1) (2014), 210–221.

[64] J. Jang, C. Y. Ahn, K. Jeon, J. Heo, D. Lee, C. Joo, J.-i. Choi and J. K. Seo, *A reconstruction method of blood flow velocity in left ventricle using color flow ultrasound*, Computational and Mathematical Methods in Medicine, **2015** (2015), 108274.

[65] G. K. Batchelor *An Introduction to Fluid Dynamics*, Cambridge Mathematical Library, Cambridge University Press, Cambridge, UK, 2000.

[66] A. Sarvazyan, T. J. Hall, M. W. Urban, M. Fatemi, S. R. Aglyamov and B. S. Garra, *An overview of elastography - an emrging branch of medical imaging*, Current Medical Imaging Reviews, **7** (2011), 255–282.

[67] J. Bercoff, M. Tanter and M. Fink, *Supersonic shear imaging: a new technique for soft tissue elasticity mapping*, IEEE Transactions on Ultrasonics, Ferroelectrics, and Frequency Control, **51** (2004), 396–409.

[68] K. Nightingale, S. McAleavey and G. Trahey, *Shear-wave generation using acoustic radiation force: in vivo and ex vivo results*, Ultrasound in Medicine & Biology, **29**(12) (2003), 1715–1723.

[69] N. C. Rouze, M. H. Wang, M. L. Palmeri and K. R. Nightingale, *Robust estimation of time-of-flight shear wave speed using a radon sum transformation*, IEEE Transactions on Ultrasonics, Ferroelectrics, and Frequency Control, **57**(12) (2010), 2662–2670.

[70] P. Song, A. Manduca, H. Zhao, M. W. Urban, J. F. Greenleaf and S. Chen, *Fast shear compounding using robust 2-d shear wave speed calculation and multi-directional filtering*, Ultrasound in Medicine & Biology, **40**(6) (2014), 1343–1355.

[71] L. Ji, J. R. McLaughlin, D. Renzi and J.-R. Yoon, *Interior elastodynamics inverse problems: shear wave speed reconstruction in transient elastography*, Inverse Problems, **19**(6) (2003), S1.

[72] J. McLaughlin and D. Renzi, *Using level set based inversion of arrival times to recover shear wave speed in transient elastography and supersonic imaging*, Inverse Problems, **22**(2) (2006), 707.

[73] J. McLaughlin and D. Renzi, *Shear wave speed recovery in transient elastography and supersonic imaging using propagating fronts*, Inverse Problems, **22**(2) (2006), 681.

[74] E. Y. Ko, *S-Detect™ in Breast Ultrasound : Initial Experience*, White Paper, WP201411-SMC-SDetect, Samsung Medison, 2014.

[75] K. Lee, J. Yoo and S. Kim, *A novel semi-automatic method for biometric measurements of the fetal brain*, White Paper, WP201412-5D-CNS, Samsung Medison, 2014.

[76] V. F. Duda and C. Köhler, *An improved quantification tool for breast ElastoScan™ : E-Breast™*, White Paper, WP201503-E-Breast™, Samsung Medison, 2015.

[77] D. J. Lim and M. H. Kim, *Experiences of Intrinsic Compression Ultrasound Elastography (E-Thyroid™) in Differentiating Benign From Malignant Thyroid Nodule*, White Paper, WP201504-E-Thyroid™, Samsung Medison, 2015.

[78] W. K. Jeong, *Liver stiffness measurement using S-Shearwave : initial experience*, White Paper, CS201505-S-Shearwave, Samsung Medison, 2015.

[79] J. H. Yoon, H. J. Chang, J. W. Kim and N. Chung *The value of multi-directional movement of carotid artery as a novel surrogate marker for acute ischemic stroke assessed by Arterial Analysis*, White Paper, WP201506-ArterialAnalysis, Samsung Medison, 2015.

[80] A. Martegani and L. Aiani, *Technological advancements improve the sensitivity of CEUS diagnostics*, White Paper, WP201507-CEUS, Samsung Medison, 2015.

[81] Samsung Applies Deep Learning Technology to Diagnostic Ultrasound Imaging, *Samsung Newsroom*, https://news.samsung.com.

[82] R. A. Castellino, *Computer aided detection (CAD): an overview*, Cancer Imaging, **5**(1) (2005), 17–19.

[83] A. Jalalian, S. B. Mashohor, H. R. Mahmud, M. I. B. Saripan, A. R. B. Ramli and B. Karasfi, *Computer-aided detection/diagnosis of breast cancer in mammography and ultrasound: a review*, Clin. Imaging, **37**(3) (2013), 420–426.

[84] K. Doi, *Computer-aided diagnosis in medical imaging: historical review, current status and future potential*, Comput. Med. Imaging Graph., **31**(4) (2007), 198–211.

[85] B. van Ginneken, C. M. Schaefer-Prokop and M. Prokop, *Computer-aided diagnosis: how to move from the laboratory to the clinic*, Radiology, **261**(3) (2011), 719–732.

[86] B. Lei, E. L. Tan, S. Chen, L. Zhuo, S. Li, D. Ni and T. Wang, *Automatic recognition of fetal facial standard plane in ultrasound image via fisher vector*, PloS one, **10**(5) (2015), e0121838.

[87] S. Joo, Y. S. Yang, W. K. Moon and H. C. Kim, *Computer-aided diagnosis of solid breast nodules: use of an artificial neural network based on multiple sonographic features*, IEEE Trans. Med. Imaging, **23**(10) (2004), 1292–1300.

[88] S. H. Kim, J. M. Lee, K. G. Kim, J. H. Kim, J. Y. Lee, J. K. Han and B. I. Choi,*Computer-aided image analysis of focal hepatic lesions in ultrasonography: preliminary results*, Abdom. Imaging, **34**(2) (2009), 183–191.

[89] R. Llobet, J. C. Pérez-Cortés, A. H. Toselli and A. Juan, *Computer-aided detection of prostate cancer* International Journal of Medical Informatics, **76**(7) (2007), 547–556.

[90] D. R. Chen, R. F. Chang, W. J. Kuo, M. C. Chen and Y. L. Huang, *Diagnosis of breast tumors with sonographic texture analysis using wavelet transform and neural networks*, Ultrasound Med. Biol., **28**(10) (2002), 1301–1310.

[91] Y. L. Huang and D. R. Chen, *Watershed segmentation for breast tumor in 2-D sonography*, Ultrasound Med. Biol., **30**(5) (2004), 625–632.

[92] D. L. Sandulescu, D. Dumitrescu, I. Rogoveanu and A. Saftoiu, *Hybrid ultrasound imaging techniques (fusion imaging)*, World J. Gastroenterol., **17**(1) (2011), 49–52.

[93] W. Wein, S. Brunke, A. Khamene, M. R. Callstrom and N. Navab, *Automatic CT-ultrasound registration for diagnostic imaging and image-guided intervention*, Med. Image Anal., **12**(5) (2008), 577–585.

[94] T. Lange, N. Papenberg, S. Heldmann, J. Modersitzki, B. Fischer, H. Lamecker and P. M. Schlag, *3D ultrasound-CT registration of the liver using combined landmark-intensity information*, Int. J. Comput. Assist. Radiol. Surg., **4**(1) (2009), 79–88.

[95] M. W. Lee, *Fusion imaging of real-time ultrasonography with CT or MRI for hepatic intervention*, Ultrasonography, **33**(4) (2014), 227–239.

[96] C. Ewertsen, A. Saftoiu, L. G. Gruionu, S. Karstrup and M. B. Nielsen, *Real-time image fusion involving diagnostic ultrasound*, Am. J. Roentgenol., **200**(3) (2013), W249–W255.

[97] B. C. Porter, D. J. Rubens, J. G. Strang, J. Smith, S. Totterman and K. J. Parker, *Three-dimensional registration and fusion of ultrasound and MRI using major vessels as fiducial markers*, IEEE Trans. Med. Imaging, **20**(4) (2001) 354–359.

[98] A. Roche, S. Pennec, G. Malandain and N. Ayache, *Rigid registration of 3-D ultrasound with MR images: a new approach combining intensity and gradient information*, IEEE Trans. Med. Imaging, **20**(10) (2001), 1038–1049.

[99] J. Jang, C. Y. Ahn, J.-I. Choi and J. K. Seo, *Inverse Problem for Color Doppler Ultrasound-Assisted Intracardiac Blood Flow Imaging*, Computational and Mathematical Methods in Medicine, **2016** (2016), 6371078.

[100] M. H. Wang, M. L. Palmeri, V. M. Rotemberg, N. C. Rouze and K. R. Nightingale, *Improving the robustness of time-of-flight based shear wave speed reconstruction methods using ransac in human liver in vivo*, Ultrasound in Medicine & Biology, **36**(5) (2010), 802–813.